ACS Sustainable Chemistry & Engineering

Research Article

pubs.acs.org/journal/ascecg

Hollow Mesoporous SiO_2–BiOBr Nanophotocatalyst: Synthesis, Characterization and Application in Photodegradation of Organic Dyes under Visible-Light Irradiation

Wei Li,[†,‡] Xiangkun Jia,[†,‡] Peitao Li,[†,‡] Baoliang Zhang,[†,‡] Hepeng Zhang,[†,‡] Wangchang Geng,[†,‡] and Qiuyu Zhang*[,†,‡]

[†]Department of Applied Chemistry, College of Science, Northwestern Polytechnical University, Xi'an 710072, China

[‡]Key Laboratory of Space Physics and Chemistry, Ministry of Education, Northwestern Polytechnical University, Xi'an 710072, China

ABSTRACT: In this paper, a novel visible-light-driven hollow $mSiO_2$–BiOBr (H-$mSiO_2$–BiOBr) nanophotocatalyst was successfully synthesized by a facile three-step method. First, the hollow mesoporous silica submicrospheres with orderly mesoporous opening structure and an independent internal cavity were synthesized by combining Stöber hydrolysis and chemical etching. Second, the hollow mesoporous silica submicrospheres were functionalized by 3-triethoxysilylpropylamine (APTES), then the amino-groups were successfully introduced into the surface of this material. Third, the BiOBr nanophotocatalyst with size of about 8–15 nm was successfully synthesized on the surface of the aforementioned amino-functionalized hollow mesoporous silica submicrospheres by solvothermal synthesis with the aid of the oriented function of the surface amino-groups. After several characterizations of the materials, the photocatalytic degradation of RhB by this H-$mSiO_2$–BiOBr nanophotocatalyst under visible-light irradiation was investigated. The experimental results revealed that the photocatalytic activity of the H-$mSiO_2$–BiOBr nanophotocatalyst was higher than that of the core–shell SiO_2@$mSiO_2$–BiOBr nanophotocatalyst under visible-light irradiation. More importantly, the nanoscale BiOBr photocatalyst, which was synthesized by controlling the addition amounts of the bismuth source, would lead to an increased band gap (1.47 eV), and it would further lead to the effective restraint for the recombination of the photoexcited electron–hole pairs. However, the rapid migration of the interface charges would enhance the photoactivity of this novel supported nanophotocatalyst significantly. Furthermore, the existence of the internal cavities of this novel nanophotocatalyst would lead to the multiple reflections of the irradiated light and effectively prolong its action time, which is also very conducive to the enhancement of the photoactivity of this supported nanophotocatalyst. Beyond that, the orderly mesoporous opening structure and the independent internal cavities can effectively facilitate the transfer of reactant molecules. This would lead to the enhanced photocatalytic performance of this novel supported BiOBr nanophotocatalyst.

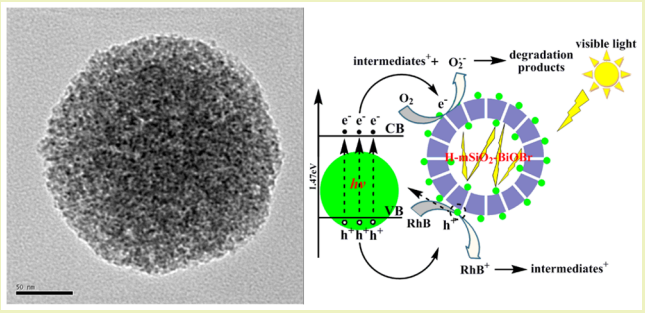

KEYWORDS: *Hollow silica, Rhodamine B, Electron–hole pair, Photocatalyst, Quantization*

INTRODUCTION

The semiconductor photocatalysis technique is an effective method to eliminate most kinds of environmental contaminations and produce hydrogen.[1−6] The development of visible-light-driven (VLD) photocatalysts has attracted more and more researchers.[7−12] Among numerous semiconductor photocatalysts, some bismuth-based photocatalysts, which generally possess wide absorbing wavelength, have exhibited superior photocatalytic activity for degrading some organic contaminants under visible-light irradiation. G. T. Chandrappa et al.[13] synthesized a nanocrystalline m-$BiVO_4$ photocatalyst by a facile solution combustion synthesis method, and this photocatalyst shows highly visible photocatalytic activity toward methylene blue degradation under sun light irradiation. P. Liu et al.[14] investigated the photoreactivity for photodegradation of 2-NAP on BiOCl nanosheets with dominant exposed (010) and (001) facets under visible-light via an exciton-free and nonsensitized mechanism, and they found that single-crystalline BiOCl nanosheets exposing (010) facets exhibit higher photoactivity due to more surface complex and more terminal bismuth atoms on the surface of BiOCl (010). Y. Zhu et al.[15] investigated a $BiTaO_4$ photocatalyst for methylene blue degradation, and research shows that the photocatalytic activity of this photocatalyst was not very high, but it can fulfill the VLD photocatalysis by modifying its surface conditions and increasing its surface area. J. Xu et al.[16] synthesized Bi_2MoO_6 nanostructures with different morphologies via a simple hydrothermal route followed by calcination, and research

Received: January 15, 2015
Revised: April 3, 2015
Published: April 27, 2015

DOI: 10.1021/acssuschemeng.5b00033
ACS Sustainable Chem. Eng. 2015, 3, 1101−1110

indicated that the photocatalyst was very effective for sulfamethazine photodegradation under solar light irradiation.

The bismuth-based photocatalyst has exhibited superior photocatalytic activity under visible-light irradiation.[17−20] However, there are still many limitations to overcome. For a semiconductor, the recombination of the photoexcited electron−hole pairs is extremely detrimental to the photocatalytic performance of the semiconductor photocatalyst, thus some better methods should be developed to eliminate the recombination of the photoexcited electron−hole pairs. Therefore, designing more efficient and more easily separable VLD semiconductor photocatalysts that meet the requirements of practical environmental applications is the primary goal of researchers in recent years. To the best of our knowledge, decreasing particle size (1−10 nm) is one of the most effective strategies, which is mainly because an enlarged energy gap would form if the particle size of the semiconductor material is small enough, thus increasing the difficulty of recombination of the photoexcited electron−hole pairs. Consequently, designing and synthesizing a novel semiconductor material with the particle size of a few nanometers has been found to be extremely meaningful for the development of excellent semiconductor photocatalysts.

In recent years, the BiOBr semiconductor, which has found to be a superior photocatalyst, has attracted increasing attention in the photocatalysis field owing to its wide absorbing wavelength.[21−25] At the same time, some BiOBr photocatalysts with a hollow structure have been reported, and some of them indeed exhibited superior performance.[26−28] Based on the aforementioned consideration, a novel and facile method was proposed to anchor the nanoscale BiOBr semiconductor photocatalyst with a particle size of 8−15 nm on the surface of amino-functionalized hollow mesoporous silica submicrospheres, and a novel VLD H-mSiO_2−BiOBr nanophotocatalyst was successfully synthesized. To the best of our knowledge, hollow silica submicrospheres, which can fulfill the multiple reflections of irradiated light in the internal cavity, can efficiently prolong the action time of irradiated light, and it is very conducive to the generation of photoexcited electrons. Simultaneously, the orderly mesoporous opening structure can facilitate the transfer of reactant molecules.[29,30] Correspondingly, it would lead to the enhanced photocatalytic performance of the BiOBr nanophotocatalyst on the surface of the hollow mesoporous silica submicrospheres. Subsequently, RhB was chosen as the target organic pollutant, and the photocatalytic activity of this H-mSiO_2−BiOBr nanophotocatalyst for degrading RhB in a water system under visible-light irradiation was investigated, and the basic photocatalytic mechanism was also discussed.

EXPERIMENTAL SECTION

Reagents and Materials. Absolute ethanol (EtOH), ammonia solution (25 wt %), tetraethoxysilane (TEOS), cetyltrimethylammonium bromide (CTAB), anhydrous sodium carbonate (Na_2CO_3), ammonium nitrate (NH_4NO_3), bismuth nitrate pentahydrate ($Bi(NO_3)_3{\cdot}5H_2O$), 3-triethoxysilylpropylamine (APTES), potassium bromide (KBr), ethylene glycol (EG), rhodamine B (RhB), potassium iodide (KI), isopropyl alcohol (IPA), *tert*-butyl alcohol (t-butanol) and *p*-benzoquinone (BQ) were purchased from J&K Chemical and were used without further treatment.

Preparation of Core−Shell SiO_2@mSiO_2/CTAB Submicrospheres. The solid silica submicrospheres were prepared by the traditional Stöber hydrolysis method. Briefly, 10 mL of ammonia solution (25 wt %) was added into the mixed solution of 200 mL of distilled water and 400 mL of absolute ethanol, then the system was stirred vigorously for 10 min. Subsequently, 50 mL of TEOS was quickly added into the aforementioned system, then the system was stirred for 6 h at the speed of 280 rpm at room temperature. After the reaction finished, the sample was separated by centrifugation at a speed of 10000 rpm and washed several times with ethanol and distilled water. Lastly, the sample was redispersed into distilled water to form the suspension with a concentration of 0.02 g/mL. Subsequently, the mesoporous silica submicrospheres with a core−shell structure were prepared by coating the silica on the surface of solid silica submicrospheres in the presence of CTAB. Briefly, the aforementioned suspension containing 2.7 g of solid silica submicrospheres was added into distilled water to form 540 mL of suspension with the aid of ultrasonication. Then, a mixed solution that consisted of 4.05 g of CTAB, 810 mL of absolute ethanol and 810 mL of distilled water was added into aforementioned system under agitation. Subsequently, 15 mL of ammonia solution (25 wt %) was added into this system, then 9.0 mL of TEOS was quickly added into this system after being stirred for 30 min, and this system was continuously stirred for 6 h. After the reaction finished, the sample was separated by centrifugation at a speed of 9000 rpm and washed several times with ethanol and distilled water, respectively. Lastly, the sample was redispersed into distilled water to form a suspension with a concentration of 0.02 g/mL.

Preparation of Hollow Mesoporous Silica Submicrospheres. The hollow mesoporous silica submicrospheres were prepared by selective etching under the protection of CTAB. Briefly, 2.5 g of the aforementioned microspheres was ultrasonically dispersed into 500 mL of distilled water, then 10 g of Na_2CO_3 was added into this system and the system was stirred vigorously for 12 h at 50 °C. After the reaction finished, the sample was separated by centrifugation at a speed of 10000 rpm and washed several times with distilled water. Subsequently, aforementioned sample was transferred into 300 mL of NH_4NO_3 ethanol solution (10 mg/mL), then the system was stirred for 24 h under the reflux device at 90 °C. Finally, the hollow mesoporous silica submicrospheres with an orderly mesoporous opening structure were successfully obtained after repeating the aforementioned operation two times.

Amino-Functionalization of Hollow Mesoporous Silica Submicrospheres. The aforementioned hollow mesoporous silica submicrospheres were ultrasonically dispersed into 150 mL of acetone, then two drops of ammonia solution (25 wt %) was added into this system under vigorous agitation. Subsequently, 2.0 mL of APTES was added into the aforementioned system, and the system was stirred vigorously for 12 h under the reflux device at 60 °C. After the reaction finished, the sample was separated by centrifugation at a speed of 10000 rpm and washed several times with ethanol and distilled water, respectively. Ultimately, the sample was dried for 12 h via vacuum freeze-drying technology.

Preparation of H-mSiO_2−BiOBr Nanophotocatalyst. The Bi^{3+} ions were anchored on the surface of amino-functionalized hollow mesoporous silica submicrospheres by the complexation between amino groups and Bi^{3+} ions, then the BiOBr nanophotocatalyst were successfully synthesized on the surface of the hollow mesoporous silica microspheres after the Bi^{3+} ions were converted to BiOBr by solvothermal synthesis. Briefly, 0.3 g of amino-functionalized hollow mesoporous silica submicrospheres was ultrasonically dispersed into 50 mL of absolute ethanol, then 0.5 g of $Bi(NO_3)_3{\cdot}5H_2O$ was added into this system. After ultrasonication for 5 min, this system was stirred slowly for 12 h. After the reaction finished, the product was separated by centrifugation at the speed of 10000 rpm and washed 2−3 times with distilled water. Subsequently, aforementioned sample was redispersed into 40 mL of EG containing 0.3 g of KBr, then the system was transferred to the Teflon-lined stainless steel autoclave with a capacity of 50 mL and kept for 4 h at 180 °C. After the reaction finished, the product was separated by centrifugation at the speed of 10000 rpm and washed several times with ethanol and distilled water, respectively. Ultimately, the as-prepared product was dried for 24 h via vacuum freeze-drying technology.

Characterization. Fourier transform-infrared (FT-IR) spectra of the samples were recorded on a PerkinElmer 580BIR spectropho-

DOI: 10.1021/acssuschemeng.5b00033
ACS Sustainable Chem. Eng. 2015, 3, 1101−1110

tometer using the KBr pellet technique. X-ray power diffraction (XRD) analysis was performed on a Bruker AXS D8-advance X-ray diffractometer with Cu Kα radiation. The morphologies and sizes of the samples were characterized using a JEOL JEM-2100F field emission transmission electron microscopy (FETEM) instrument. X-ray photoelectron spectroscopy (XPS) data were collected to examine the chemical states of the photocatalyst with an Axis Ultra instrument (Kratos Analytical, Manchester, U.K.) under ultrahigh vacuum conditions ($<10^{-6}$ Pa) and using a monochromatic Al Kα X-ray source (1486.6 eV). N_2 adsorption/desorption isotherms were obtained on a TriStar II 20 apparatus. The Brunauer–Emmett–Teller (BET) method was used to calculate the specific surface area based on the adsorption branches. UV–vis diffuse reflectance spectra (DRS) were obtained using a Shimadzu UV-3600 spectrometer by using $BaSO_4$ as a reference at room temperature.

Photocatalytic Performance Tests. The photocatalytic activity of the as-prepared H-mSiO_2–BiOBr nanophotocatalyst was evaluated respectively by catalyzing the photodegradation of RhB in aqueous solution at room temperature under visible light irradiation with one 500 W xenon lamp (CHF-XM500, light intensity = 600 mW/cm^2) located 20 cm away from the reaction solution. To make sure that the photocatalytic reaction was really driven by visible light, all the UV lights with wavelengths less than 420 nm were removed by a glass filter (JB-420). In a typical reaction, 0.2 g of as-prepared supported photocatalyst was dispersed into 100 mL of dye aqueous solution (20 mg/L). Before light irradiation, the suspension was stirred for 30 min in the dark to reach the adsorption equilibrium of dye molecules on the surface of the nanophotocatalyst. Then, 5 mL of reaction solution was extracted to determine the concentration of the dye in aqueous solution by UV–vis spectroscopy. In this study, the core–shell mesoporous silica submicrospheres supported BiOBr nanophotocatalyst, which was synthesized by the same method, was used as the reference catalyst to catalyze the photodegradation of RhB in aqueous solution under the same conditions as the aforementioned operation, respectively. The dye aqueous solution without photocatalyst irradiated by visible light was used as the blank experiment. After the experiment was finished, the catalyst was collected by centrifugal separation and respectively washed several times with ethanol and distilled water, then the recovered catalyst underwent further purification treatment in a dialysis bag for 12 h. Finally, the photodegradation experiment catalyzed by the recovered catalyst was carried out repeatedly according to the aforementioned operation steps.

Radical Trapping Experiments. For detecting the active species during photocatalytic reactivity, hydroxyl radicals (·OH), superoxide radical ($O_2^{\bullet-}$) and holes (h^+) were investigated by adding 1.0 mM IPA (a quencher of ·OH),[21] 1.0 mM BQ (a quencher of $O_2^{\bullet-}$) and 1.0 mM NaI (a quencher of h^+),[9] respectively. The method was similar to the former photocatalytic activity test.

RESULTS AND DISCUSSION

Characterization of Photocatalyst. To investigate the morphology transformation of the materials in the synthetic process, the materials obtained in every step were characterized by TEM, and Figure 1 displays the corresponding TEM images. The silica cores with a diameter of 170 nm, which were synthesized by the traditional Stöber hydrolysis method, show a good spherical structure and monodispersed in diameter (Figure 1a,b). After being coated with mesoporous silica, the obvious core–shell structure can be observed, which exhibits very uniform distribution, and its shell thickness is about 40 nm (Figure 1c,d). Obviously, the core–shell mesoporous silica microspheres still maintain good spherical and monodispersed diameters after mesoporous silica coating. Subsequently, the inner silica cores were removed by the chemical etching technique, and the hollow mesoporous silica submicrospheres were successfully obtained. Figure 1e,f shows that every silica microsphere has an internal cavity, and the diameter of the

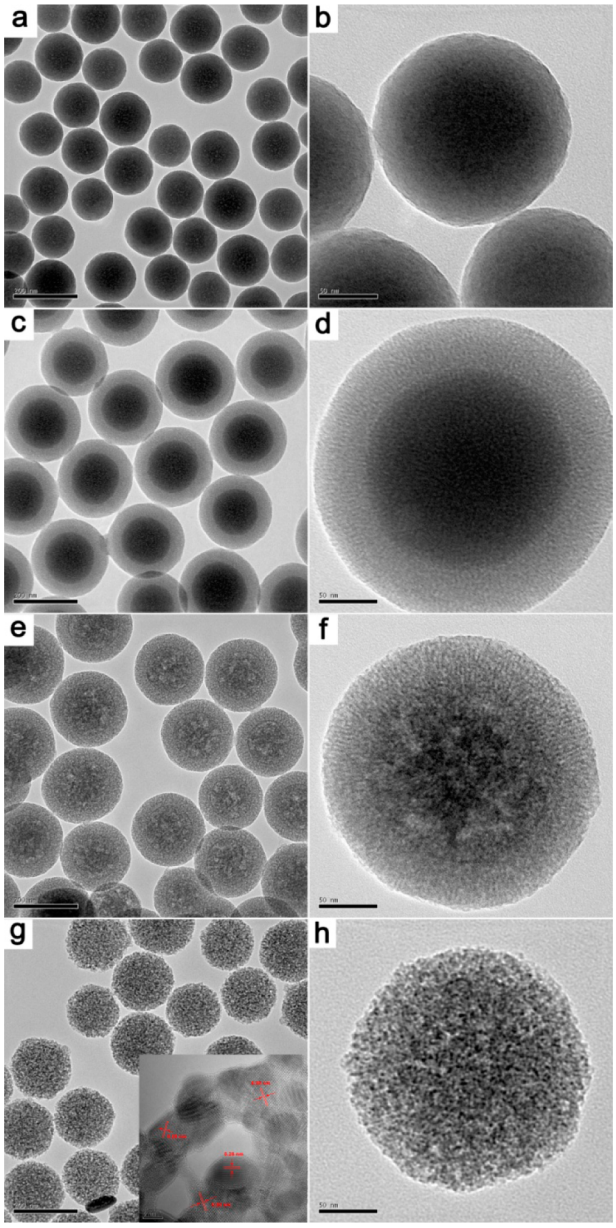

Figure 1. TEM images of silica internal cores (a and b), core–shell mesoporous silica submicrospheres (c and d), hollow mesoporous silica submicrospheres (e and f) and H-mSiO_2–BiOBr nanophotocatalyst (g and h). The inset of panel g is the HRTEM image of H-mSiO_2–BiOBr nanophotocatalyst. All the scale bars of the TEM images for panels a, c, e and g are 200 nm and 50 nm for panels b, d, f, and h, and it is 5 nm for the HRTEM image (inset of panel g).

cavity is about 150 nm. In addition, the particle size of the hollow mesoporous silica submicrospheres is about 230 nm, and it is less than that of core–shell mesoporous silica submicrospheres. The reason for the decrease of the diameter is that the particles had shrinked to some extent after the internal cores were removed. Subsequently, the BiOBr nanoparticles were anchored onto the surface of the hollow mesoporous silica submicrospheres, then the H-mSiO_2–BiOBr nanophotocatalyst with an internal cavity was successfully obtained. Figure 1g,h shows that there was no aggregation to be observed, and the BiOBr photocatalyst was immobilized on the surface of the hollow mesoporous silica submicrospheres in the ultrafine nanosize form. A high resolution transmission electron

DOI: 10.1021/acssuschemeng.5b00033
ACS Sustainable Chem. Eng. 2015, 3, 1101–1110

microscopy (HRTEM) image (the inset in Figure 1g) of H-mSiO$_2$−BiOBr nanophotocatalyst shows clear lattice fringes, indicating its high crystallinity, which is a characteristic of photocatalysts with high activities. The clear lattice fringes of the interplane were about 0.28 nm, which were in accordance with (110) planes of the tetragonal system of BiOBr. In addition, Figure 1g shows that the diameter of the hollow mesoporous silica microspheres had become 200 nm (previous 230 nm) for treatment under high temperature and high pressure in the solvothermal process.

Figure 2a displays the N_2 adsorption/desorption isotherms of hollow mesoporous silica submicrospheres and the H-mSiO$_2$−BiOBr nanophotocatalyst, and both exhibit representative type H1 isotherms. The BET surface area and the single-point total pore volume for hollow mesoporous silica submicrospheres came out to be 1015.4 m^2/g and 0.86 cm^3/g, and 189.8 m^2/g and 0.37 m^3/g for the H-mSiO$_2$−BiOBr nanophotocatalyst, respectively. The obvious decrease in the BET surface area and pore volume after the immobilization of the BiOBr nanophotocatalyst can be observed, which should be caused by the morphology change of the submicrostructures after being treated at high temperatures and pressures. As shown in Figure 2b, the average Barrett−Joyner−Halenda (BJH) pore diameter of the hollow mesoporous silica submicrospheres and H-mSiO$_2$−BiOBr nanophotocatalyst calculated from the desorption branch of the isotherms was determined to be 3 and 7 nm, respectively. Obviously, the significant increase of the pore size is also a key factor for the decrease of the BET surface area, and it was also caused by the treatment at high temperatures and pressures. Gratifyingly, the high surface area and appropriate pore size of the H-mSiO$_2$−BiOBr nanophotocatalyst can increase the effective contact area and facilitate the transfer of reactant molecules, which would contribute to the enhancement in photocatalytic activity to some extent.

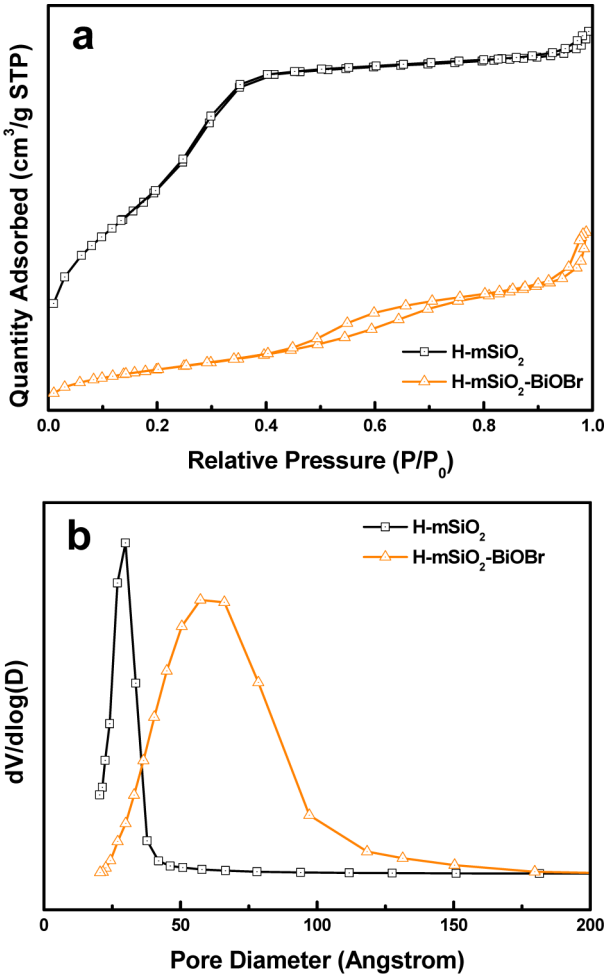

Figure 2. N_2 adsorption/desorption isotherms (a) and diameter distribution (b) of the samples.

XRD was employed to determine the crystallographic phase of the samples, and the XRD patterns of the hollow mesoporous silica submicrospheres and the H-mSiO$_2$−BiOBr nanophotocatalyst are displayed in Figure 3. The broad peak around 2θ = 24° can be attributed to the characteristic diffraction peak of amorphous silica (Figure 3a). In Figure 3b, the diffraction peaks at 27.2°, 32.3°, 40.2°, 46.2° and 55.7° can be attributed to the reflection of the (101), (110), (112), (200) and (212) planes, respectively. All diffraction peaks are identical to the structure of the tetragonal phase BiOBr (JCPDS card No. 09-0393), and the intense and sharp diffraction peaks suggested that the as-synthesized BiOBr nanophotocatalyst on the surface of the hollow mesoporous silica submicrospheres is well-crystallized.

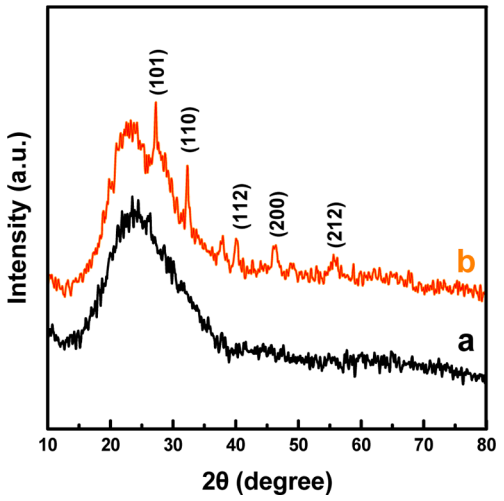

Figure 3. XRD spectra of hollow mesoporous silica submicrospheres (a) and H-mSiO$_2$−BiOBr nanophotocatalyst (b).

XPS characterization provides further insight into the assessment of the surface composition of H-mSiO$_2$−BiOBr nanophotocatalyst. The XPS spectrum in Figure 4a reveals that the surface of this supported nanophotocatalyst consisted of O, C, Bi and Br, and it indicates that the BiOBr photocatalyst should have been anchored on the surface of the hollow mesoporous silica submicrospheres. Two peaks at 159.2 and 164.5 eV in Figure 4b were respectively attributed to $Bi_{4f7/2}$ and $Bi_{4f5/2}$, which indicates the existence of Bi^{3+} in BiOBr. Two small peaks at 160.2 and 165.5 eV should be caused by the complexation between Bi atoms and amino-groups on the surface of the hollow mesoporous silica submicrospheres. The $Br_{3d5/2}$ and $Br_{3d3/2}$ peaks (Figure 4c) were associated with the binding energies at 68.4 and 69.4 eV, respectively. Two peaks at 531.9 and 534.8 eV should be fitted with the characteristic peaks of O_{1s} in BiOBr and in SiO_2, and two peaks at 533.8 and 535.6 eV should be assigned to the characteristic peaks of O_{1s} in PVP adsorbed on the surface of the H-mSiO$_2$−BiOBr

DOI: 10.1021/acssuschemeng.5b00033
ACS Sustainable Chem. Eng. 2015, 3, 1101−1110

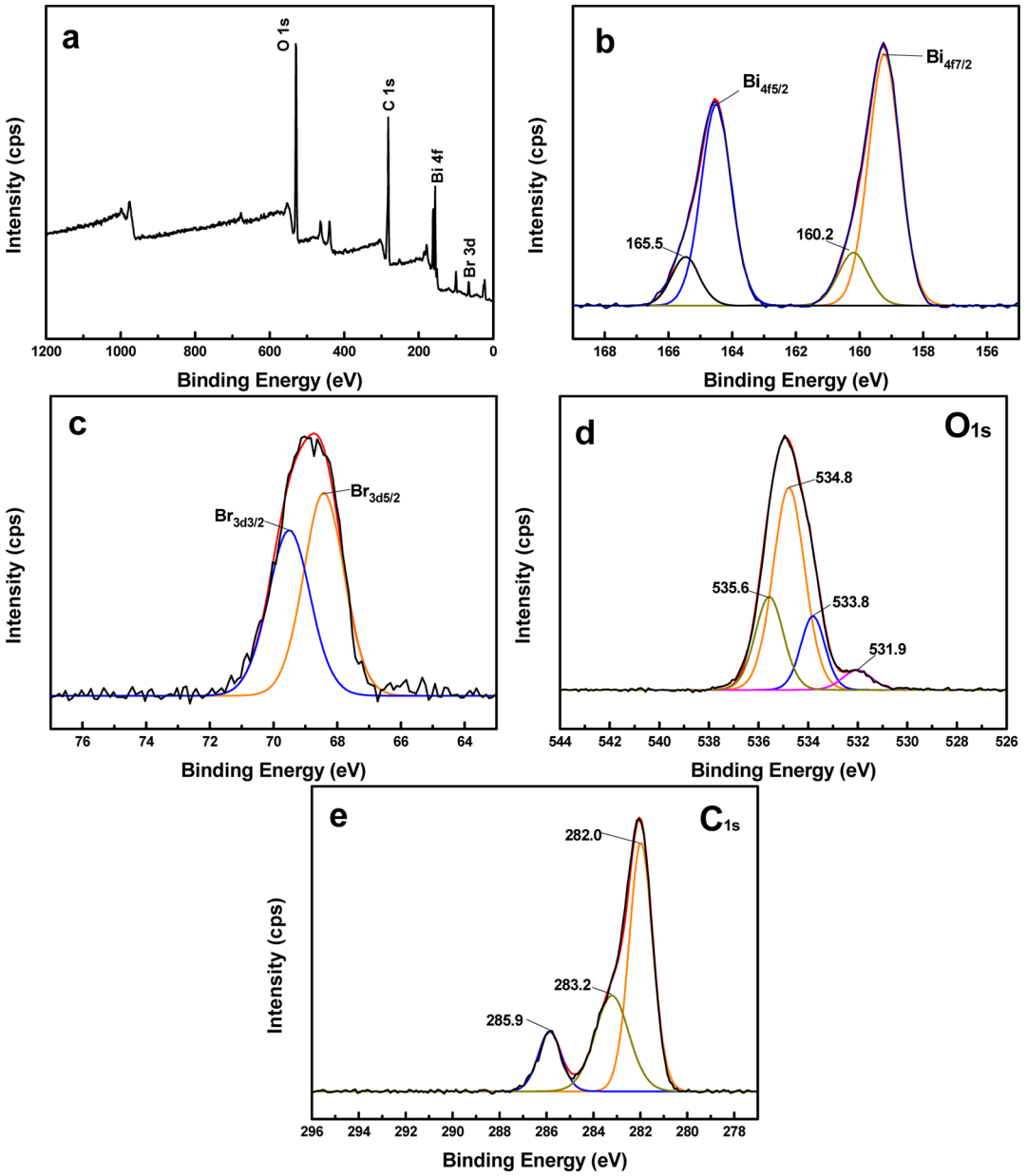

Figure 4. XPS spectra of H-mSiO$_2$−BiOBr nanophotocatalyst.

nanophotocatalyst (Figure 4d). In addition, three peaks at 285.9, 283.2 and 282.0 eV in Figure 4e should be attributed to the characteristic of C_{1s} in APTES grafted on the surface of the hollow mesoporous silica submicrospheres. This demonstrates well that the pure BiOBr nanophotocatalyst had been successfully anchored on the surface of the hollow mesoporous silica submicrospheres.

For a VLD semiconductor photocatalyst, the optical absorption property is a key factor to determine its photocatalytic activity.[31] Figure 5a shows the UV−vis diffuse reflection spectra (DRS) of the as-prepared H-mSiO$_2$−BiOBr nanophotocatalyst and SiO$_2$@mSiO$_2$−BiOBr nanophotocatalyst. Obviously, both the absorption edges of two supported BiOBr nanophotocatalysts were located in the visible-light range (≫420 nm), and the H-mSiO$_2$−BiOBr nanophotocatalyst exhibited stronger absorption than that of the SiO$_2$@mSiO$_2$−BiOBr nanophotocatalyst. The enhanced absorption should be caused by the introduction of the internal cavities. The band gap (E_g) of the semiconductors can be obtained from eq 1:[19]

$$\alpha h\nu = A(h\nu - E_g)^{n/2} \quad (1)$$

In the aforementioned formula, α, ν and A are absorption coefficient, light frequency and proportionality constant, respectively. n can be determined by the type of optical transition of a semiconductor (i.e., n = 1 for direct transition and n = 4 for indirect transition). For BiOBr, the n value is 1.[32] The E_g values of the two supported BiOBr nanophotocatalysts were obtained from the plots of $(\alpha h\nu)^2$ versus photon energy ($h\nu$) (Figure 5b), and was 1.56 eV for the SiO$_2$@mSiO$_2$−BiOBr nanophotocatalyst, and 1.47 eV for the H-mSiO$_2$−BiOBr nanophotocatalyst, respectively. These results imply that the visible light response of this novel H-mSiO$_2$−BiOBr nanophotocatalyst had been enhanced by the nanocrystallization of BiOBr photocatalyst and the synergistic effect of the internal cavities of hollow mesoporous silica submicrospheres,

DOI: 10.1021/acssuschemeng.5b00033
ACS Sustainable Chem. Eng. 2015, 3, 1101−1110

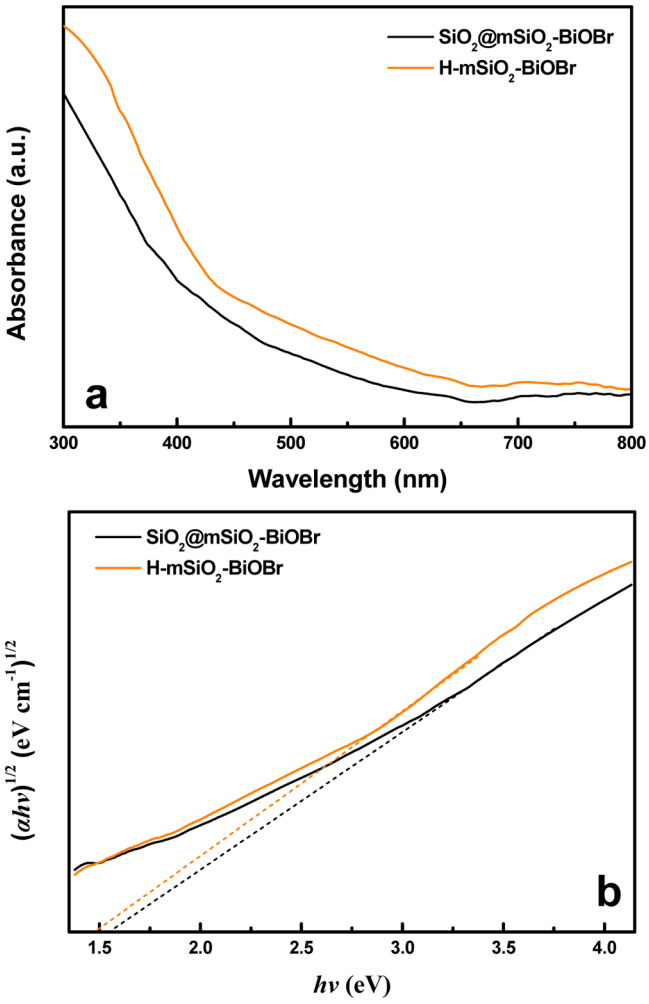

Figure 5. (a) UV−vis diffuse reflection spectra and (b) plot of $(\alpha h\nu)^{1/2}$ versus $h\nu$ of the as-prepared supported BiOBr nanophotocatalysts.

and a lower band gap is very beneficial for electronic transitions, which subsequently results in enhanced photocatalytic activity.

Photocatalytic Performance. Rhodamine B (RhB), which showed a major absorption band at 557 nm, was chosen as a representative target organic pollutant to evaluate the photocatalytic performance of as-prepared H-$mSiO_2$−BiOBr nanophotocatalyst. Figure 6a shows that the saturated adsorption of the SiO_2@$mSiO_2$−BiOBr nanophotocatalyst and H-$mSiO_2$−BiOBr nanophotocatalyst is 5.48% and 58.94%, respectively. It indicates that the presence of the internal cavity can significantly enhance the adsorption ability of the supported nanophotocatalyst to the target organic pollutant, which should be caused by the concentration gradient between the internal cavity and the bulk solution. Figure 6b displays the corresponding photocatalytic degradation kinetic curves. Blank test confirmed that the self-photolysis of RhB could be negligible, and the H-$mSiO_2$−BiOBr nanophotocatalyst exhibited higher photocatalytic activity than that of the core−shell SiO_2@$mSiO_2$−BiOBr nanophotocatalyst. In particular, for the presence of the concentration gradient and catalysis of the H-$mSiO_2$−BiOBr nanophotocatalyst, the RhB molecules would quickly transform into the activated intermediates for the photosensitization under visible-light irradiation, so the concentration of the RhB solution would first display a sharp decline before 10 min. By combining with Figure 6d, the point at 10 min in Figure 6b should be a transition point. Compared with the black curve, the green curve shows an obvious blue shift, and its peak height had been decreased significantly (in Figure 6d). A shift in the absorption band toward the blue region can be attributed to the step-by-step de-ethylation process.[33] Subsequently, the peak height of the blue curve (in Figure 6d) would increase to some extent, and the blue shift can still be observed. After 20 min, the peak height gradually weakened to the end point, which indicates that the photodegradation plays a primary role at this stage until the activated intermediates were degraded perfectly. Furthermore, it can also be demonstrated by comparing the digital photos in Figure 6c,d. Obviously, the color of the RhB solution would turn to yellow-green from the original pink, then it would further turn to colorless (digital photos in Figure 6d). In addition, the degradation kinetics were also investigated by fitting the experimental data to the Langmuir−Hinshelwood model (Figure 6e). It is easy to see that the photodegradation of RhB by the SiO_2@$mSiO_2$−BiOBr nanophotocatalyst obeyed first-order kinetics well, but it basically obeyed second-order kinetics by the H-$mSiO_2$−BiOBr nanophotocatalyst for the presence of the hollow structure. Simultaneously, the rate constants corresponding to SiO_2@$mSiO_2$−BiOBr and H-$mSiO_2$−BiOBr are also calculated by $-\ln(c_t/c_0) = kt$ and $-\ln(c_t/c_0) = kt^2 + b$, and are about 0.0036 min^{-1} and 0.1339 min^{-2}, respectively.

The recycled experiments were carried out to evaluate the photostability of the H-$mSiO_2$−BiOBr nanophotocatalyst under visible-light irradiation. After every 100 min photocatalytic reaction, the separated nanophotocatalyst was washed several times with distilled water, then it was redispersed into the fresh RhB aqueous solution. The concentration change of RhB during each cycle is shown in Figure 7. It shows that after six cycling runs of photodegradation of RhB, the photocatalytic ability of the H-$mSiO_2$−BiOBr nanophotocatalyst did not show obvious loss. More importantly, after six cycles, the morphology of this H-$mSiO_2$−BiOBr nanophotocatalyst was almost unchanged (Figure 7b), which indicates that the H-$mSiO_2$−BiOBr nanophotocatalyst is a stable photocatalyst in the photocatalysis reaction system.

Photocatalytic Mechanism. To investigate the main active species involved in the photodegradation of RhB in the presence of the novel H-$mSiO_2$−BiOBr nanophotocatalyst under visible-light irradiation, a series of photodegradation experiments with the addition of different scavengers were investigated in an attempt to elucidate the photocatalytic mechanism, and the corresponding degradation kinetic curves are displayed in Figure 8. As shown as the orange curve in Figure 8, when IPA (·OH scavenger) was added into the degradation system, the photodegradation activity only had a slight decrease, and the obvious photosensitization could still be observed in the illumination of 10 min. It demonstrates that the ·OH radicals are not the main active species. However, when any one of KI (h^+ scavenger), BQ ($O_2^{\bullet-}$ scavenger) and t-butanol (e^- acceptor) was added into the degradation system, extremely low photodegradation activity would be observed, and the aforementioned photosensitization could not be observed anymore (as Figure 8). This indicates that h^+, $O_2^{\bullet-}$ and e^- each play an important role in the degradation process. In the H-$mSiO_2$−BiOBr nanophotocatalyst system, the possible photocatalytic mechanisms are proposed as

DOI: 10.1021/acssuschemeng.5b00033
ACS Sustainable Chem. Eng. 2015, 3, 1101−1110

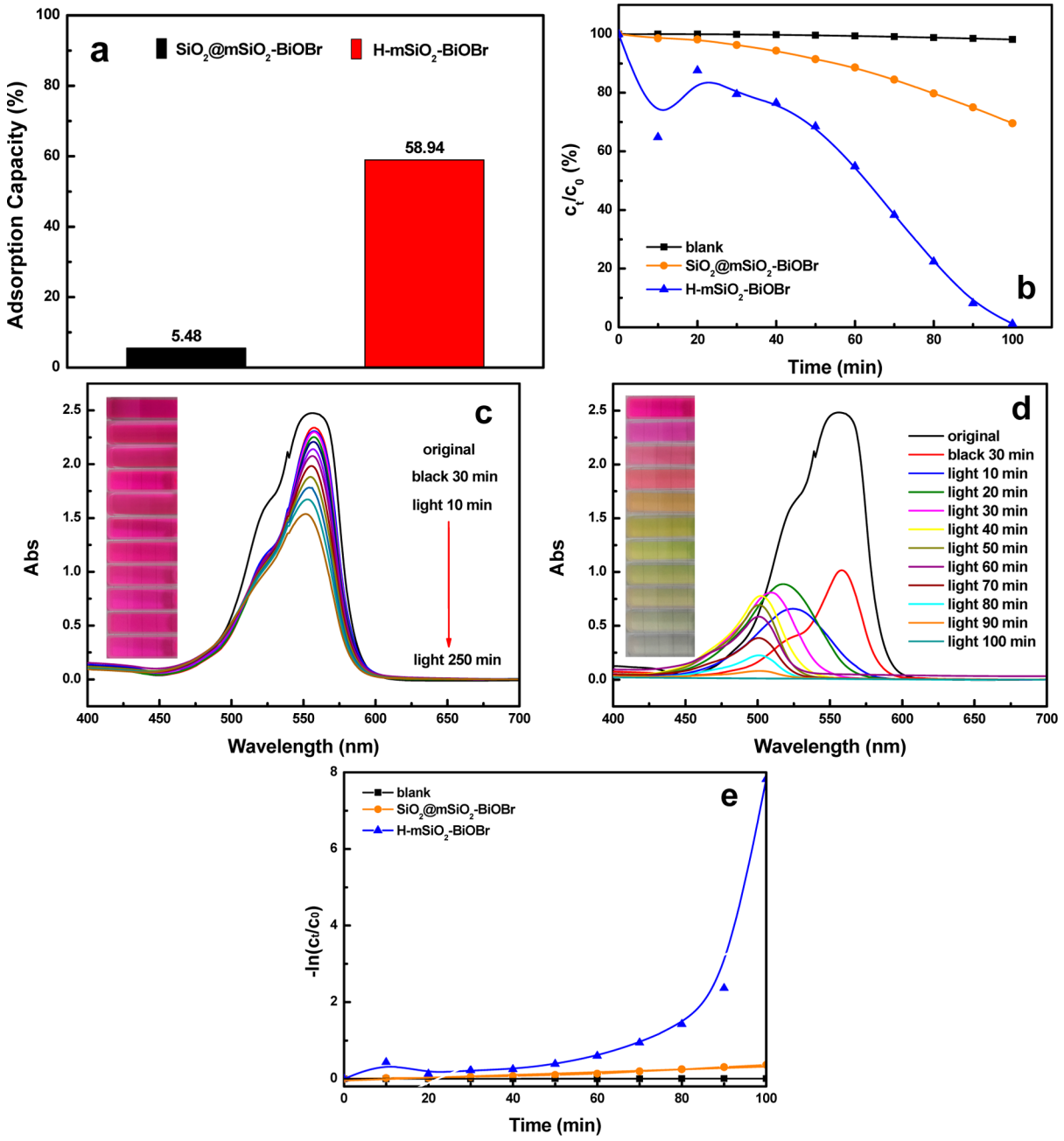

Figure 6. Saturated adsorption of the photocatalyst for RhB (a), photocatalytic degradation activity for RhB under visible-light (λ > 420 nm) irradiation (b), UV−vis absorption spectra changes of RhB (20 mg/L, 100 mL) in the presence of the SiO_2@mSiO_2−BiOBr (0.2 g) (c) and H-mSiO_2−BiOBr (0.2 g) (d) under visible-light irradiation, and the corresponding fitted kinetics of panel b according to the Langmuir−Hinshelwood model (e).

$$\text{photocatalyst} + h\nu \rightarrow \text{photocatalyst}\ (h^+ + e^-) \quad (2)$$

$$RhB + h^+ \rightarrow RhB^+ \rightarrow \text{intermediates}^+ \quad (3)$$

$$O_2 + e^- \rightarrow O_2^{\cdot -} \quad (4)$$

$$\text{intermediates}^+ + O_2^{\cdot -} \rightarrow \cdots \rightarrow \text{degradation products} \quad (5)$$

Under visible-light irradiation, the reaction is initiated with the excitation of the H-mSiO_2−BiOBr nanophotocatalyst, resulting in the promotion of electrons (e^-) from the valence band (VB) to the conduction band (CB) of the BiOBr semiconductor and the generation of holes (h^+) in the VB (eq 2). Then, the holes react with RhB molecules to form the intermediates$^+$ (eq 3). At the same time, oxygen molecules capture electrons to form $O_2^{\bullet -}$ radicals (eq 4), then the intermedicates$^+$ react with $O_2^{\bullet -}$ radicals to form the ultimate degradation products (eq 5).

For a semiconductor, the quantum size effect (QSE) would happen when the particle size is in the range 1−10 nm.[4] A key feature of this effect is that the increased band gap would lead to the effective restraint for the recombination of the photoexcited electron−hole pairs. Furthermore, the existence of the internal cavities of the carriers would lead to multiple reflections of the irradiated light and enhance the absorption ability of the irradiated light to some extent.[34] More

DOI: 10.1021/acssuschemeng.5b00033
ACS Sustainable Chem. Eng. 2015, 3, 1101−1110

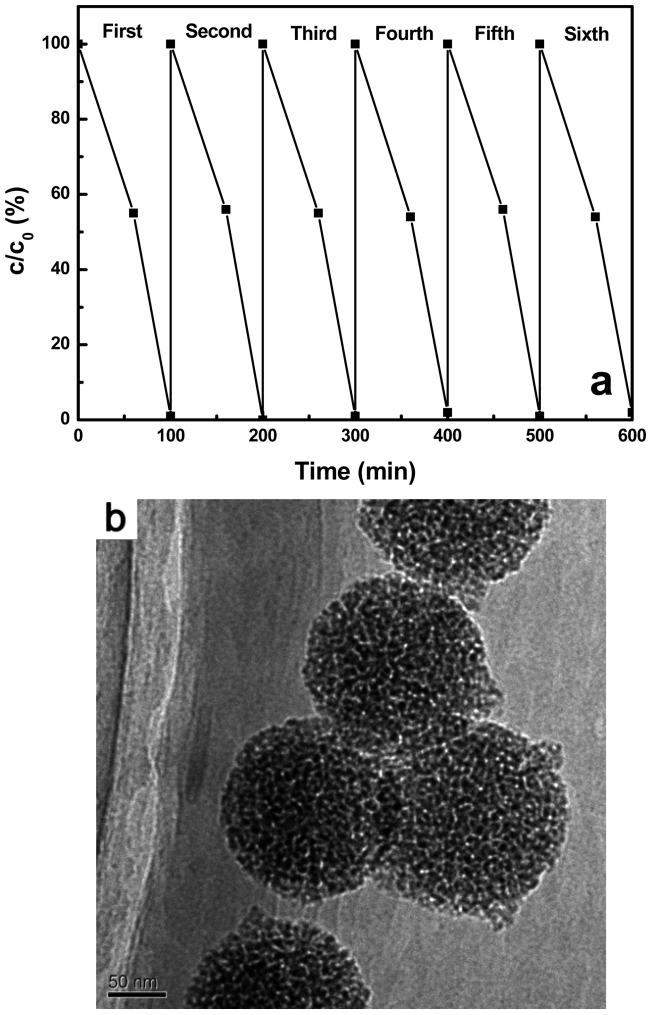

Figure 7. (a) Photodegradation of RhB during the recycled experiments. The initial RhB concentration was 20 mg/L, and the dose of the hollow $mSiO_2$−BiOBr nanophotocatalyst was 2.0 g/L. (b) TEM image of H-$mSiO_2$−BiOBr nanophotocatalyst after being used six times.

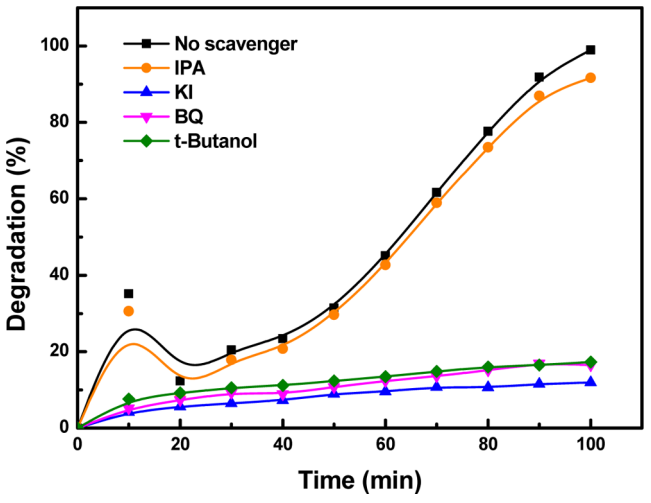

Figure 8. Effects of different scavengers on degradation of RhB in the presence of H-$mSiO_2$−BiOBr nanophotocatalyst under visible-light irradiation.

importantly, synthesizing the BiOBr nanoparticles with an appropriate size and dispersion on the surface of hollow mesoporous silica submicrospheres would be very effective for the enhancement of the photocatalytic activity of the photocatalyst, which is because this novel structure can fulfill the rapid transfer of electrons in the interfaces and enhance visible region absorption to some extent.[35] Generally, there are three possible reaction mechanisms in dye photodegradation in the presence of a semiconductor photocatalyst: a photolysis process, a dye photosensitization process and a photocatalytic process.[36] Here, the whole photodegradation process should contain at least three steps: the adsorption process, the dye photosensitization process and the photocatalytic process. In the adsorption process, RhB molecules in the bulk solution would first be enriched on the surface and in the internal cavities of the H-$mSiO_2$−BiOBr nanophotocatalyst by the concentration gradient effect for the presence of the internal cavity. In the photosensitization process, the RhB molecules on the surface of the nanophotocatalyst would quickly transform into the activated intermediates$^+$ after capturing the holes, and more and more activated intermediates$^+$ would be generated with the extend of the illumination time. At the same time, the photoexcited electrons on the surface of the photocatalyst would react with O_2 molecules to produce the $O_2^{\bullet-}$ radicals that can work as a main active species for RhB photodegradation. In the photocatalytic process, the activated intermediates$^+$ would react with $O_2^{\bullet-}$ radicals to transform into the ultimate degradation products (CO_2 and H_2O) (Figure 9).

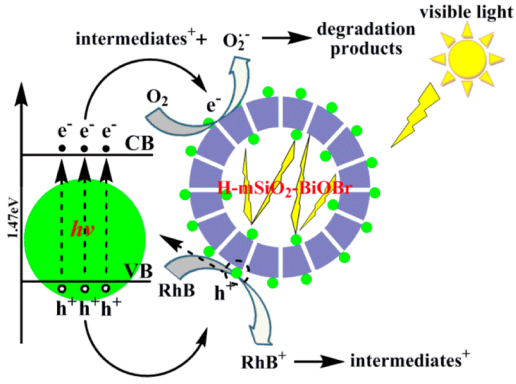

Figure 9. Schematic illustration of the proposed photocatalytic mechanism of the H-$mSiO_2$−BiOBr nanophotocatalyst under visible-light irradiation.

CONCLUSION

In this paper, a novel VLD H-$mSiO_2$−BiOBr nanophotocatalyst was successfully synthesized by a facile three-step method. First, the hollow mesoporous silica submicrospheres with an orderly mesoporous opening structure and an independent internal cavity were synthesized by combining Stöber hydrolysis and chemical etching. Second, the hollow mesoporous silica microspheres were functionalized by APTES, then the amino-groups were successfully introduced into the surface of this material. Third, a BiOBr photocatalyst with a size range of about 8−15 nm was successfully synthesized by solvothermal synthesis with the aid of the oriented function of the surface amino-groups. Subsequently, RhB was chosen as the target organic pollutant, and photocatalytic degradation experiments

DOI: 10.1021/acssuschemeng.5b00033
ACS Sustainable Chem. Eng. 2015, 3, 1101−1110

in the presence of the H-mSiO$_2$−BiOBr nanophotocatalyst under visible-light irradiation were investigated. The experimental results revealed that the photocatalytic activity of this novel H-mSiO$_2$−BiOBr nanophotocatalyst was more superior than that of the core−shell SiO$_2$@mSiO$_2$−BiOBr nanophotocatalyst under visible-light irradiation. More importantly, the nanoscale BiOBr photocatalyst would lead to the increased band gap (1.47 eV), which would further lead to the effective restraint for the recombination of the photoexcited electron−hole pairs. However, the fast migration of the interface charges would enhance the photoactivity of this novel supported nanophotocatalyst significantly. Furthermore, the existence of the internal cavities of this novel nanophotocatalyst would lead to multiple reflections of the irradiated light and effectively prolong its action time, which is also very conducive to the enhancement of the photoactivity of this novel supported nanophotocatalyst. Simultaneously, the orderly mesoporous opening structure can effectively facilitate the transfer of reactant molecules. Therefore, it would lead to the enhanced photocatalytic performance of the BiOBr nanophotocatalyst on the surface of the hollow mesoporous silica submicrospheres.

AUTHOR INFORMATION

Corresponding Author

*Qiuyu Zhang. Phone: +86-029-88431675. Fax: +86-029-88431675. E-mail: qyzhang@nwpu.edu.cn.

Notes

The authors declare no competing financial interest.

ACKNOWLEDGMENTS

The authors are grateful for the financial support provided by the National Natural Science Foundation of China (No. 51173146 and No. 21201140), basic research fund of Northwestern Polytechnical University (3102014JCQ01094, 3102014ZD).

REFERENCES

(1) Liang, K.; Tay, B. K.; Kupreeva, O. V.; Orekhovskaya, T. I.; Lazarouk, S. K.; Borisenko, V. E. Fabrication of double-walled titania nanotubes and their photocatalytic activity. *ACS Sustainable Chem. Eng.* **2014**, *2*, 991−995.

(2) Wang, H.; Zhang, L.; Chen, Z.; Hu, J.; Li, S.; Wang, Z.; Liu, J.; Wang, X. Semiconductor heterojunction photocatalysts: Design, construction, and photocatalytic performances. *Chem. Soc. Rev.* **2014**, *43*, 5234−5244.

(3) Cani, D.; Pescarmona, P. P. Macroscopic TiO$_2$-SiO$_2$ porous beads: Efficient photocatalysts with enhanced reusability for the degradation of pollutants. *J. Catal.* **2014**, *311*, 404−411.

(4) Yu, X.; Shavel, A.; An, X.; Luo, Z.; Ibáñez, M.; Cabot, A. Cu$_2$ZnSnS$_4$-Pt and Cu$_2$ZnSnS$_4$-Au heterostructured nanoparticles for photocatalytic water splitting and pollutant degradation. *J. Am. Chem. Soc.* **2014**, *136*, 9236−9239.

(5) Hong, D.; Yamada, Y.; Sheehan, M.; Shikano, S.; Kuo, C.-H.; Tian, M.; Tsung, C.-K.; Fukuzumi, S. Mesoporous nickel ferrites with spinel structure prepared by an aerosol spray pyrolysis method for photocatalytic hydrogen evolution. *ACS Sustainable Chem. Eng.* **2014**, *136*, 2588−2594.

(6) Sun, Y.; Sun, J.; Long, J. R.; Yang, P.; Chang, C. J. Photocatalytic generation of hydrogen from water using a cobalt pentapyridine complex in combination with molecular and semiconductor nanowire photosensitizers. *Chem. Sci.* **2013**, *4*, 118−124.

(7) Yu, C.; Li, G.; Kumar, S.; Yang, K.; Jin, R. Phase transformation synthesis of novel Ag$_2$O/Ag$_2$CO$_3$ heterostructures with high visible light efficiency in photocatalytic degradation of pollutants. *Adv. Mater.* **2014**, *26*, 892−898.

(8) Wang, T.; Li, C.; Ji, J.; Wei, Y.; Zhang, P.; Wang, S.; Fan, X.; Gong, J. Reduced graphene oxide (rGO)/BiVO$_4$ composites with maximized interfacial coupling for visible light photocatalysis. *ACS Sustainable Chem. Eng.* **2014**, *2*, 2253−2258.

(9) Sin, J.-C.; Lam, S.-M.; Satoshi, I.; Lee, K.-T.; Mohamed, A. R. Sunlight photocatalytic activity enhancement and mechanism of novel europium-doped ZnO hierarchical micro/nanospheres for degradation of phenol. *Appl. Catal., B* **2014**, *148*, 258−268.

(10) Dong, H.; Chen, G.; Sun, J.; Li, C.; Yu, Y.; Chen, D. A novel high-efficiency visible-light sensitive Ag$_2$CO$_3$ photocatalyst with universal photodegradation performances: Simple synthesis, reaction mechanism and first-principles study. *Appl. Catal., B* **2013**, *134*, 46−54.

(11) Dong, S.; Sun, J.; Li, Y.; Yu, C.; Li, Y.; Sun, J. ZnSnO$_3$ hollow nanospheres/reduced graphene oxide nanocomposites as high-performance photocatalysts for degradation of metronidazole. *Appl. Catal., B* **2014**, *144*, 386−393.

(12) Stamatis, N.; Antonopoulou, M.; Hela, D.; Konstantinou, I. Photocatalytic degradation kinetics and mechanisms of antibacterial triclosan in aqueous TiO$_2$ suspensions under simulated solar irradiation. *J. Chem. Technol. Biotechnol.* **2014**, *89*, 1145−1154.

(13) Nagabhushana, G. P.; Nagaraju, G.; Chandrappa, G. T. Synthesis of bismuth vanadate: Its application in H$_2$ evolution and sunlight-driven photodegradation. *J. Mater. Chem. A* **2013**, *1*, 388−394.

(14) Weng, S.; Pei, Z. X.; Zheng, Z.; Hu, J.; Liu, P. Exciton-free, nonsensitized degradation of 2-naphthol by facet-dependent BiOCl under visible light: Novel evidence of surfacestate photocatalysis. *ACS Appl. Mater. Interfaces* **2013**, *5*, 12380−12386.

(15) Shi, R.; Lin, J.; Wang, Y.; Xu, J.; Zhu, Y. Visible-light photocatalytic degradation of BiTaO$_4$ photocatalyst and mechanism of photocorrosion suppression. *J. Phys. Chem. C* **2010**, *114*, 6472−6477.

(16) Guo, C.; Xu, J.; Wang, S.; Zhang, Y.; He, Y.; Li, X. Photodegradation of sulfamethazine in an aqueous solution by a bismuth molybdate photocatalyst. *Catal. Sci. Technol.* **2013**, *3*, 1603−1611.

(17) Dong, F.; Li, Q.; Sun, Y.; Ho, W.-K. Noble metal-like behavior of plasmonic Bi particles as a cocatalyst deposited on (BiO)$_2$CO$_3$ microspheres for efficient visible light photocatalysis. *ACS Catal.* **2014**, *4*, 4341−4350.

(18) Nell, A.; Getsoian, A. B.; Werner, S.; Kiwi-Minsker, L.; Bell, A. T. Preparation and characterization of high-surface-area Bi$_{(1-x)/3}$V$_{1-x}$Mo$_x$O$_4$ Catalysts. *Langmuir* **2014**, *30*, 873−880.

(19) Hu, R.; Xiao, X.; Tu, S.; Zuo, X.; Nan, J. Synthesis of flower-like heterostructured β-Bi$_2$O$_3$/Bi$_2$O$_2$CO$_3$ microspheres using Bi$_2$O$_2$CO$_3$ self-sacrifice precursor and its visible-light-induced photocatalytic degradation of *o*-phenylphenol. *Appl. Catal., B* **2015**, *163*, 510−519.

(20) Moniz, S. J. A.; Blackman, C. S.; Carmalt, C. J.; Hyett, G. MOCVD of crystalline Bi$_2$O$_3$ thin films using a single-source bismuth alkoxide precursor and their use in photodegradation of water. *J. Mater. Chem.* **2010**, *20*, 7881−7886.

(21) Ye, L.; Liu, J.; Jiang, Z.; Peng, T.; Zan, L. Facets coupling of BiOBr-g-C$_3$N$_4$ composite photocatalyst for enhanced visible-light-driven photocatalytic activity. *Appl. Catal., B* **2013**, *142*, 1−7.

(22) Jiang, G.; Wang, R.; Wang, X.; Xi, X.; Hu, R.; Zhou, Y.; Wang, S.; Wang, T.; Chen, W. Novel highly active visible-light-induced photocatalysts based on BiOBr with Ti doping and Ag decorating. *ACS Appl. Mater. Interfaces* **2012**, *4*, 4440−4444.

(23) Zhang, L.; Wang, W.; Sun, S.; Sun, Y.; Gao, E.; Zhang, Z. Elimination of BPA endocrine disruptor by magnetic BiOBr@SiO$_2$@Fe$_3$O$_4$ photocatalyst. *Appl. Catal., B* **2014**, *148*, 164−169.

(24) Wei, X.-X.; Chen, C.-M.; Guo, S.-Q.; Guo, F.; Li, X.-M.; Wang, X.-X.; Cui, H.-T.; Zhao, L.-F.; Li, W. Advanced visible-light-driven photocatalyst BiOBr-TiO$_2$-graphene composite with graphene as a nano-filler. *J. Mater. Chem. A* **2014**, *2*, 4667−4675.

(25) Huo, Y.; Zhang, J.; Miao, M.; Jin, Y. Solvothermal synthesis of flower-like BiOBr microspheres with highly visible-light photocatalytic performances. *Appl. Catal., B* **2012**, *111*, 334−341.

DOI: 10.1021/acssuschemeng.5b00033
ACS Sustainable Chem. Eng. 2015, 3, 1101−1110

(26) Xia, J.; Yin, S.; Li, H.; Xu, H.; Xu, L.; Xu, Y. Improved visible light photocatalytic activity of sphere-like BiOBr hollow and porous structures synthesized via a reactable ionic liquid. *Dalton Trans.* **2011**, *40*, 5249−5258.
(27) Cheng, H.; Huang, B.; Wang, Z.; Qin, X.; Zhang, X.; Dai, Y. One-pot miniemulsion-mediated route to BiOBr hollow microspheres with highly efficient photocatalytic activity. *Chem.—Eur. J.* **2011**, *17*, 8039−8043.
(28) Jiang, G.; Wang, X.; Wei, Z.; Li, X.; Xi, X.; Hu, R.; Tang, B.; Wang, R.; Wang, S.; Wang, T.; Chen, W. Photocatalytic properties of hierarchical structures based on Fe-doped BiOBr hollow microspheres. *J. Mater. Chem. A* **2013**, *1*, 2406−2410.
(29) Ge, M.; Liu, L.; Chen, W.; Zhou, Z. Sunlight-driven degradation of Rhodamine B by peanut-shaped porous $BiVO_4$ nanostructures in the H_2O_2-containing system. *CrystEngComm* **2012**, *14*, 1038−1044.
(30) Li, W.; Zhang, B.; Li, X.; Zhang, H.; Zhang, Q. Preparation and characterization of novel immobilized Fe_3O_4@SiO_2@mSiO_2-Pd(0) catalyst with large pore-size mesoporous for Suzuki coupling reaction. *Appl. Catal., A* **2013**, *459*, 65−72.
(31) Tang, J.; Zou, Z.; Ye, J. Efficient photocatalytic decomposition of organic contaminants over $CaBi_2O_4$ under visible-light irradiation. *Angew. Chem., Int. Ed.* **2004**, *43*, 4463−4466.
(32) Sun, S. M.; Wang, W. Z.; Zhou, L.; Xu, H. L. Efficient methylene blue removal over hydrothermally synthesized starlike $BiVO_4$. *Ind. Eng. Chem. Res.* **2009**, *48*, 1735−1739.
(33) Di, J.; Xia, J.; Yin, S.; Xu, H.; Xu, L.; Xu, Y.; He, M.; Li, H. Preparation of sphere-like g-C_3N_4/BiOI photocatalysts via a reactable ionic liquid for visible-light-driven photocatalytic degradation of pollutants. *J. Mater. Chem. A* **2014**, *2*, 5340−5351.
(34) Peng, J.; Zhao, L.; Zhu, X.; Sun, Y.; Feng, W.; Gao, Y.; Wang, L.; Li, F. Hollow silica nanoparticles loaded with hydrophobic phthalocyanine for near-infrared photodynamic and photothermal combination therapy. *Biomaterials* **2013**, *34*, 7905−7912.
(35) Xu, H.; Yan, J.; Xu, Y.; Song, Y.; Li, H.; Xia, J.; Huang, C.; Wan, H. Novel visible-light-driven AgX/graphite-like C_3N_4 (X = Br, I) hybrid materials with synergistic photocatalytic activity. *Appl. Catal., B* **2013**, *129*, 182−193.
(36) Wang, Q.; Hui, J.; Huang, Y.; Ding, Y.; Cai, Y.; Yin, S.; Li, Z.; Su, B. The preparation of BiOCl photocatalyst and its performance of photodegradation on dyes. *Mater. Sci. Semicond. Process.* **2014**, *17*, 87−93.

DOI: 10.1021/acssuschemeng.5b00033
ACS Sustainable Chem. Eng. 2015, 3, 1101−1110